In severe COVID-19, SARS-CoV-2 induces a chronic, TGF-β-dominated adaptive immune response

Marta Ferreira-Gomes[1,*], Andrey Kruglov[1,2,3,*], Pawel Durek[1,*], Frederik Heinrich[1,*], Caroline Tizian[4,5,6,*], Gitta Anne Heinz[1,*], Anna Pascual-Reguant[1,7], Weijie Du[1], Ronja Mothes[1,8], Chaofan Fan[1], Stefan Frischbutter[9], Katharina Habenicht[10], Lisa Budzinski[1], Justus Ninnemann[1], Peter K. Jani[1], Gabriela Guerra[1], Katrin Lehmann[1], Mareen Matz[11], Lennard Ostendorf[1,8], Lukas Heiberger[1], Hyun-Dong Chang[1], Sandy Bauherr[1,], Marcus Maurer[9], Günther Schönrich[12], Martin Raftery[12], Tilmann Kallinich[1,5,13], Marcus Alexander Mall[5,13,14], Stefan Angermair[15], Sascha Treskatsch[15], Thomas Dörner[1,7], Victor Max Corman[12], Andreas Diefenbach[4,5,6], Hans-Dieter Volk[11,16], Sefer Elezkurtaj[17], Thomas H. Winkler[10], Jun Dong[1], Anja Erika Hauser[1,7], Helena Radbruch[8,*], Mario Witkowski[4,5,6,*], Fritz Melchers[1,*], Andreas Radbruch[1,*], Mir-Farzin Mashreghi[1,11,*,#]

[1]Deutsches Rheuma-Forschungszentrum (DRFZ), an Institute of the Leibniz Association, 10117, Berlin, Germany.
[2]Belozersky Institute of Physico-Chemical Biology and Biological Faculty, M.V. Lomonosov Moscow State University, Moscow 119234, Russia.
[3]Center for Precision Genome Editing and Genetic Technologies for Biomedicine, Engelhardt Institute of Molecular Biology, Russian Academy of Sciences, Moscow, 119991, Russia.
[4]Laboratory of Innate Immunity, Department of Microbiology and Infection Immunology, Charité-Universitätsmedizin Berlin, 12203 Berlin, Germany.
[5]Berlin Institute of Health (BIH), 10178 Berlin, Germany.
[6]Mucosal and Developmental Immunology, Deutsches Rheuma-Forschungszentrum, Charitéplatz 1, 10117 Berlin, Germany
[7]Department of Rheumatology and Clinical Immunology, Charité-Universitätsmedizin Berlin, corporate member of Freie Universität Berlin, Humboldt-Universität zu Berlin, and Berlin Institute of Health, Berlin, Germany.
[8]Department of Neuropathology, Charité-Universitätsmedizin Berlin, corporate member of Freie Universität Berlin, Humboldt-Universität zu Berlin, and Berlin Institute of Health, Berlin, Germany.
[9]Dermatological Allergology, Department of Dermatology and Allergy, Charité-Universitätsmedizin Berlin, corporate member of Freie Universität Berlin, Humboldt-Universität zu Berlin, and Berlin Institute of Health, Berlin, Germany.
[10]Friedrich-Alexander-University Erlangen-Nuremberg, Erlangen, Germany.
[11] BIH Center for Regenerative Therapies (BCRT), Charité Universitätsmedizin Berlin, Berlin, Germany.
[12]Institute of Virology, Charité-Universitätsmedizin Berlin, corporate member of Freie Universität Berlin, Humboldt-Universität zu Berlin, and Berlin Institute of Health, Berlin, Germany.
[13]Department of Pediatric Pulmonology, Immunology and Critical Care Medicine, Charité-Universitätsmedizin Berlin, corporate member of Freie Universität Berlin, Humboldt-Universität zu Berlin, and Berlin Institute of Health, Berlin, Germany.
[14]German Centre for Lung Research (DZL), associated partner site, Berlin, Germany
[15]Department of Anesthesiology and Intensive Care Medicine, Campus Benjamin Franklin, Charité - Universitätsmedizin Berlin, Corporate Member of Freie Universität Berlin, Humboldt-Universität zu Berlin, and Berlin Institute of Health, Berlin, Germany.

[16]Institute of Medical Immunology, Charité - Universitätsmedizin Berlin, Corporate Member of Freie Universität Berlin, Humboldt-Universität zu Berlin, and Berlin Institute of Health, Berlin, Germany.
[17]Institute of Pathology, Charité - Universitätsmedizin Berlin, Corporate Member of Freie Universität Berlin, Humboldt-Universität zu Berlin, and Berlin Institute of Health, Berlin, Germany.

*equal contribution

#Correspondence: Dr. Mir-Farzin Mashreghi, +493028460752, mashreghi@drfz.de

Abstract
Here we have analyzed the dynamics of the adaptive immune response triggered by SARS-CoV-2 in severely affected COVID-19 patients, as reflected by activated B cells egressing into the blood, at the single cell level. Early on, before seroconversion in response to SARS-CoV-2 spike protein, activated peripheral B cells displayed a type 1 interferon-induced gene expression signature. After seroconversion, activated B cells lost this signature, expressed IL-21- and TGF-β-induced gene expression signatures, and mostly IgG1 and IgA1. In the sustained immune reaction of the COVID-19 patients, until day 59, activated peripheral B cells shifted to expression of IgA2, reflecting instruction by TGF-β. Despite the continued generation of activated B cells, those cells were not found in the lungs of deceased COVID-19 patients, nor did the IgA2 bind to dominant antigens of SARS-CoV-2. In severe COVID-19, SARS-CoV-2 thus triggers a chronic immune reaction distracted from itself and instructed by TGF-β.

To analyze the adaptive immune response triggered by SARS-CoV-2 in severely affected COVID-19 patients, we initially focused on activated B lymphocytes of the peripheral blood, considering them as biosensors of the ongoing immune reaction and effectors of humoral immunity(Mei et al., 2010; Odendahl et al., 2005). To do so, we established a cohort (characterized in Supplementary Fig. 1a) of 11 COVID-19 intensive care unit (ICU) patients, admitted to the ICU according to the QuickSOFA score of clinical parameters, the POST-SAVE-Concept of the state of Berlin(Wiesner et al., 2020). We analysed samples from 6 patients within the first week after ICU admission, all except from one (patient #11, day 7) being seronegative for the spike (S) protein of SARS-CoV-2, and from 7 patients who had been in the ICU for more than a week (9 to 59 days) and who were seropositive (IgG) for SARS-CoV-2 S protein. Note that 3 of the patients were analysed both at early and late time points (patient #1, 3, 8). 3 healthy controls were also included. $CD27^{high}CD38^{high}$ cells of the B cell lineage were enriched from peripheral blood by MACS and FACS (Supplementary Fig. 1b). The frequencies of $CD27^{high}CD38^{high}$ B cells were significantly elevated in the peripheral blood of COVID-19 patients compared to healthy controls (Fig. 1a). From the enriched cells we generated single cell transcriptomes and B cell receptor (BCR) repertoires. According to their transcriptomes, cells were clustered by Uniform Manifold Approximation and Projection for Dimension Reduction (UMAP)(Becht et al., 2018). UMAP defined 6 distinct clusters of $CD27^{high}CD38^{high}$ B cells in the patients and healthy controls analyzed (Fig.1b,c,d), although not all patients and controls showed cells in all clusters (Fig. 1e,f, Supplementary Fig 1c). Cluster 1 contained predominantly $CD19^{+}CD20^{+}CD27^{+}$ experienced B lymphocytes, with a gene expression signature

resembling that of resting B lymphocytes(Riedel et al., 2020) (Fig. 1b,d). Cells of cluster 6 were *IRF4*^{high}*PRDM1*^{high} late plasmablasts and plasma cells(Sciammas et al., 2006) (Fig. 1b,d). Cells of cluster 2 and 3 represented *CD19*$^{+}$*CD27*$^{+}$*CD38*$^{+}$ activated B cells, with cells of cluster 2 expressing *MIKI67*, i.e. proliferating, and cells of cluster 3 not expressing *MKI67*, marking them as cells in proliferative rest (Fig. 1b,d). Cells of clusters 4 and 5 were also activated *CD19*$^{+}$*CD27*$^{+}$*CD38*$^{+}$ B cells, but distinct from those of clusters 2 and 3 by expression of interferon (IFN) signature genes, like IFIT1(Fensterl and Sen, 2015) (Fig. 1b,d). While cells of cluster 4 did express MKI67, cells of cluster 5 did not. Of note, cells of cluster 2 and 4 as well as 3 and 5 are transcriptionally related (Fig.1c). Cells of clusters 2 to 5 lost expression of *MS4A1* (CD20) but expressed *IRF4* and *PRDM1*, as well as *CD40*, *HLA-DR*, *IGJ*, and integrins and chemokine receptors important for migration into mucosal tissue(Stein and Nombela-Arrieta, 2005) (Fig. 1d, Supplementary Fig. 1d), thus characterizing them as activated B cells on their way to differentiate into antibody-secreting plasma cells. Cells of clusters 1, 2 and 3 were dominant in healthy individuals, who showed very few circulating plasma cells (cluster 6) and no activated B cells expressing IFN-induced signature genes (cluster 5) (Fig. 1e,f). Cells expressing IFN-induced signature genes were the most abundant in the six “early” ICU COVID-19 patients, who also showed a prominent population of plasma cells (cluster 6), but only very few experienced, resting B cells (cluster 1). In the 8 patients who had been in the ICU for more than 7 days (including 3 who were also analyzed at early time points), activated B cells with an IFN-induced gene signature were not present (Fig. 1e,f). Instead, prominent populations of clusters 2 and 3 became apparent. Circulating plasma cells were still abundant, while only a few experienced B cells were captured and sequenced (Fig. 1e,f). Taken together, patients recently admitted to the ICU showed a prominent egress of activated, IFN-driven B cells and plasma cells into the peripheral blood, while in patients with prolonged ICU stays (more than 7 days), circulating activated B cells and plasma cells were still prominent, but the underlying immune reaction was no longer driven by IFNs.

All patients who had been in the ICU for more than 7 days had in their serum SARS-CoV-2 spike (S) protein-specific IgM, and IgG antibodies. Only four of them had S-specific IgA1 antibodies and only one showed detectable titers of S-specific IgA2 antibodies (Fig 2a, Supplementary Fig. 2a-d). Specific antibodies were measured both by ELISA and by cytometric serology using human embryonic kidney (HEK) cells transformed to express SARS-CoV-2 S protein. Both assays correlated significantly (Supplementary Fig. 2e). This indicated that SARS-CoV-2 had induced a significant humoral immune reaction, including the activation of SARS-CoV-2 specific B cells, antibody class switching to IgG and IgA, and their differentiation into plasma cells. Antibody classes characterize the immune reaction underlying the egress of activated B cells and plasma cells into the blood. Activated B cells of COVID-19 patients expressed most prominently IgM, IgG1, IgA1, IgG2 and IgA2 antibodies (Fig. 2b). Instruction to switch to IgG1 is controlled by the cytokines IL-10 and IL-21(Fujieda et al., 1996; Pene et al., 2004), while switching to IgG2 is controlled by IFN-γ(Kitani and Strober, 1993), and switching to IgA1 and IgA2 by TGF-β(Islam et al., 1991). Considering the arrangement of the genes for antibody heavy chain constant regions on the chromosome(Radbruch et al., 1986), sequential switching from IgG1 to IgA is possible, also from IgA1 to IgG2, but not the reverse, IgA2 being the 3’ terminal gene for the antibody heavy chain locus. Activated B cells expressing IgM, *i.e*. not yet class switched, were most frequent in healthy controls and in the COVID-19 patients early at ICU, at frequencies of up to 18% (Fig. 2c). In patients

hospitalized in the ICU for longer, IgM^+ cells were below or around 5%. Activated B cells expressing IgG2, reflecting switch instruction by IFNs, were most frequent in patient #2, i.e. early on in ICU and before seroconversion, and in patient #8. Activated B cells expressing IgG1 were rare (2%) among healthy donors, but frequent in COVID-19 patients, ranging from 17 to 38%. Interestingly, in all patients except patient #7, these $IgG1^+$ cells define coherent subpopulations within clusters 2, 3, 4 and 5, which also contain the IgA1-expressing cells. The third most abundant antibody class found in the COVID-19 patients was IgA2. IgA2 expressing cells formed a subpopulation within cluster 3, different from the IgG1/IgA1 expressing cells in patients #3 to #9. These data allow us to conclude that in early stages of severe COVID-19 the switch instruction of IFN-instructed B cells (clusters 4 and 5) had been dominated by IL-21 and TGF-β, leading most cells to express IgG1 or IgA1. In prolonged ICU stay, switch instruction by TGF-β appears to be continuing, inducing the cells to switch towards the most distal of all antibody classes, IgA2, resulting in a significant (p=0.008) increase in the frequency of IgA2 expressing activated B cells when comparing patients early and late in ICU (Fig. 2b). Even on a systemic level, serum concentrations of IgA2 increase significantly over time in ICU, while IgG and IgA1 levels do not (Fig. 2d, Supplementary Fig. 2f). Continued switch instruction by TGF-β is also evident from the expression of Iα1 and Iα2 switch transcripts in the activated B cells of clusters 2 and 3 of patients #3 to #8 (Supplementary Fig. 3a,b). These switch transcripts reflect switch instruction and precede switch recombination, both on the active and on the allelically excluded Ig heavy chain locus(Jung et al., 1993; Lorenz et al., 1995). The impact of prolonged TGF-β signaling on activated B cells of cluster 3 is not only evident from the switch transcripts, but also from gene sets obtained from previously published data on human IL-2/IL-21-activated B cells treated for different time periods with TGF-β in the presence of IL-6 and IL-21(Stephenson et al., 2019). While activated B cells of cluster 2 and 4 were enriched for genes of IL-2/IL-21-activated B cells expanded for 6 days (Supplementary Fig. 3d), cells of cluster 4 and 5 showed enrichment for genes which are expressed in IL-2/IL-21-activated B cells in the presence of IL-6/IL-21 and IFN-α for additional 12h (Supplementary Fig. 3d). Activated B cells of cluster 3 obtained from patients #3 to #6 are enriched for genes that are characteristic for B cells that have been stimulated with IL-6/IL-21 and TGF-β for 12h, and are predominantly of IgG1 isotype (Fig. 2c,e). In contrast, activated B cells of cluster 3 from patients #7 to #9 showed an enrichment of genes obtained from activated B cells treated for 24 and 48h with IL-6/IL-21 and TGF-β, and express predominantly IgA1 and IgA2 (Fig. 2c,e). These gene sets include genes known to be induced by Stat3 and SMADs(Hall et al., 2003; Itoh et al., 2018; Kee et al., 2001; Kwon et al., 2009; Mellado et al., 1998; Mokrani et al., 2014; Shaim et al., 2017; Tomcik et al., 2015)(Supplementary Fig. 1d).

The termination of interferon-instruction of activated B cells parallels the dynamics of serum concentrations of type II IFNs, which were prominent in the plasma at the early time points, but weaning later in the 7 patients monitored (Fig. 2f). Conversely, concentrations of TGF-β were increasing with time (Fig. 2f). Accordingly, activated B cells of patients beyond day 7 expressed the signature genes of IL2/IL21-activated B cells which had been further stimulated with additional TGF-β (Fig. 2e). In summary, severely affected COVID-19 patients show a continued immune reaction with egress of activated B cells and plasma cells into the blood, which initially is controlled by IFNs, IL-21 and TGF-β, and later on predominantly by TGF-β.

The obvious involvement of IL-21 in the instruction of activated B cells of COVID-19 patients points to cognate B cell activation by follicular helper T (Tfh)/Th17 cells, which are the main producers of IL-21(Parrish-Novak et al., 2000). Moreover, enhanced TGF-β expression has been described to be a hallmark of continued activation of Th17 cells (Gutcher et al., 2011; Lee et al., 2012). TGF-β could also be provided by other sources, like regulatory T cells (Tregs) or neutrophils from the peripheral blood and airway tissue(Chu et al., 2000). Interestingly, it has been reported that during SARS-CoV infection, cause of the SARS outbreak in 2003, TGF-β1 was increased in mucosal tissues(He et al., 2006). Furthermore, SARS-CoV nucleoprotein (NP), which is 90% homologous to SARS-CoV-2 NP(Grifoni et al., 2020), can directly activate SMAD3, enhancing TGF-β-mediated gene expression(Zhao et al., 2008), which could also include TGF-β itself (Van Obberghen-Schilling et al., 1988). Therefore, we focused our next analysis on SARS-CoV-2 reactive $CD4^+$ T lymphocytes. We analyzed transcriptomes and TCR repertoires of single T cells from 3 patients who had been at ICU for 13, 29 and 32 days, respectively (Supplementary Fig. 4a), and who were seropositive for IgM and IgG, and one of them also for IgA (Fig. 3a), focusing on their expression of *IL21* and *TGFB1*. To this end, PBMCs were stimulated for 6 hours with a mixed peptide pool representing the SARS-CoV-2 spike glycoprotein (S), the membrane glycoprotein (M), and the nucleocapsid phosphoprotein (NP). Reactive $CD4^+$ T lymphocytes expressing CD137 or CD154 were enriched magnetically, representing antigen-experienced regulatory and effector cells, respectively (Fig. 3b, Supplementary Fig. 4b)(Bacher et al., 2016). While we were able to isolate only very few of such cells from a healthy donor, frequencies of antigen-reactive $CD4^+$ T cells among total $CD4^+$ T cells in the three patients were 3.5%, 1.5% and 4.9%, respectively (Supplementary Fig. 4b). UMAP clustering identified two major populations expressing *CD3E*: Tregs expressing *FOXP3* and *IKZF2* (Helios) and Tfh cells expressing *ICOS* and *PDCD1* (Fig. 3c,d). After 6h of antigenic stimulation Tfh cells expressed *CD40LG, IFNg, IL2, TNF*, but lacked the expression of *IL17, IL10* and all type 2 T helper cell-related cytokines (Fig 3d). T helper (Th) cells expressing *IL21* (1 to 10%), *TGFB1* (2.9 to 9.5%) and *IL21* plus *TGFB1* (0.3 to 3.5%) were as frequent among the SARS-CoV-2-reactive Th cells as among measles-reactive Th cells of a healthy control (2%, 6%, 0.6%, Fig 3e). No significant numbers of *IL21* and/or *TGFB1* expressing SARS-CoV-2 reactive Th cells could be isolated from a healthy control (Fig. 3e, Supplementary Fig. 4b). Of note, the TCR repertoires of SARS-CoV-2 specific Tregs and Tfh cells are unique and not overlapping, with only 13 out of 1473 analyzed TCR clones being present in both subsets, a phenomenon that has also been observed for aero-antigen-specific Tregs and conventional T cells (Bacher et al., 2016). Taken together, these data demonstrate that severely affected COVID-19 patients have significant populations of circulating, SARS-CoV-2-experienced $CD4^+$ T lymphocytes which are imprinted to express IL-21 and TGF-β, and thus qualify as instructors of B cell activation in continued, SARS-CoV-2-triggered immune reactions.

While it is obvious that the continued immune reactions of ICU COVID-19 patients are triggered by SARS-CoV-2, it is less clear whether they are also directed (exclusively) against SARS-CoV-2. The antigen-receptor repertoire of the activated B cells is rather oligoclonal (Supplementary Fig. 4c) and shows somatic hypermutation, as demonstrated here for selected, expanded clonal families (Supplementary Fig. 4d), a hallmark of cognate interaction with $CD4^+$ T cells (Cyster and Allen, 2019). Metadata on prominent clonal families of each patient are available as supplementary information. Noteworthy is the fact that while all late ICU patients

showed serum IgG, and one third also IgA1 antibodies specific for the S protein of SARS-CoV-2, only one (patient #4) was seropositive for S-specific IgA2 (Fig. 2a), suggesting that the continued immune reaction to SARS-CoV-2 did not contribute significantly to humoral immunity against the virus. In line with this, only 3/13 patients (#8, #10 and #14) had detectable titers of neutralizing antibodies late in ICU. Furthermore, none of 5 cloned BCRs , representing 5 different expanded clones of activated B cells (Supplementary Fig. 4d), recognize the SARS-CoV-2 S or NP. This finding is distinctly different from reported evidence for Influenza, where about 50% of the circulating activated B cells are hemagglutinin-specific (Wrammert et al., 2011).

If not relevant for systemic humoral immunity to SARS-CoV-2, the prolonged immune reaction and switch to IgA2 could contribute to local immunity at mucosal surfaces(Vu Van et al., 2016). All analyzed activated B cells and plasma cells expressed the J chain required to dimerize IgA and excrete it into the mucosal lumen (*IGJ*; Supplementary Fig. 1d)(Johansen et al., 2000). They also expressed CCR10 and ITGAE which could guide them into mucosal tissue (Supplementary Fig. 1d). It is therefore quite surprising, that in the lungs of 3 deceased COVID-19 patients (see Supplementary Fig. 5a for patient demographics and disease history), IgA or IgA2 expressing activated B cells and plasma cells were rare, even when the patient had been affected by sepsis due to bacterial superinfection, while IgA, and in particular IgA2, -expressing B cells were prominent in the lungs of patients with COVID-19-unrelated pneumonia (Fig. 4a,b,c, Supplementary Fig. 5b). In line with this observation, among cells isolated from broncheoalveolar lavage (BAL) fluid of patient #1, at day 59 (5459 cells), and patient #9, at days 31 (433 cells) and 46 (2723 cells) after ICU admission, only 42 cells in patient #1 on day 59, 10 cells in patient #9 on day 31 and 143 cells on day 46 were B cells (Fig. 4d,e, Supplementary Fig. 5c,d,e). The BAL was composed mainly of *CD14* expressing cells and T cells, which expressed *CD40LG*, *IFNG* and *TGFB1* and few of them *IL21* (Fig. 4d,e, Supplementary Fig. 5d,e). In patient #9 we observed an increase of cell infiltration on day 46 as compared to day 31. The majority of these cells expressed *TGFB1* (Fig. 4e).

In conclusion, we demonstrate here that severely affected COVID-19 patients which required prolonged ICU care show a continued immune reaction reflected by egress of activated B lymphocytes into the blood. This immune reaction is initially controlled by IFNs, IL-21 and TGF-β, which target antibody class switching to IgG1 and IgA1. At later time points IFN is no longer involved, and the immune reactions are controlled by IL-21 and TGF-β, which in the end drives activated B cells to switch to the terminal antibody class IgA2. Such cells do not relocate to the lung and they contribute little to humoral immunity to SARS-CoV-2. The specificities of the antibodies generated remain to be identified, but most of them are not specific for the spike protein, its receptor binding domain (RBD) or NP. Whether or not the antibodies generated in the continued immune reactions of COVID-19 patients in the ICU are harmless, or whether they may even cause detrimental immunopathology remains to be shown. Therapeutic targeting of TGF-β may be a way to ameliorate severe COVID-19, especially, when considering the fibrosis-inducing capacity of TGF-β(Polak et al., 2020).

Material and Methods

Human Donors

The recruitment of study subjects was conducted in accordance with the Ethics Committee of the Charité (EA 1/144/13 with EA 1/075/19 and EA 2/066/20) and was in compliance with the Declaration of Helsinki. Four healthy adults (3 male and 1 female; average age 47 ± 7 (SEM)) and 13 COVID-19 patients (7 male and 6 female; average age 74 ± 11 (SEM)) with either documented disease history or exposure through natural SARS-CoV-2 infection that were verified by the levels of antigen-reactive antibody IgG titers.

Sample collection and preparation

Four to twenty milliliters of peripheral blood were drawn from each donor into Vacutainer® K2E (EDTA) Plus Blood Collection Tubes (BD Biosciences, Plymouth, U.K.). Blood samples were subjected to immediate preparation. In cases where cell enrichment was not performed directly from blood, mononuclear cells were isolated by density gradient centrifugation using Ficoll-Hypaque (Sigma-Aldrich). Serum samples were collected on the same time into Vacutainer® SST™ tubes (BD Biosciences, Plymouth, U.K.). Alternatively, the plasma fraction was isolated from EDTA blood. Bronchoalveolar lavage was passed via 70 mcm cell strainer and lymphoid cells were isolated using anti-human CD45 microbeads (Miltenyi Biotec) and live cells were further sorted using a MA900 Multi-Application Cell Sorter (Sony Biotechnology). Both the serum and plasma samples were stored at -20°C until further use.

B cell isolation from peripheral blood

B cells were enriched from peripheral blood using StraightFrom® Whole Blood CD19 MicroBeads (Miltenyi Biotec) according to manufacturer's instructions. Enriched cells were incubated with Fc Blocking Reagent (Milteniy Biotec) following manufacturer's instructions and subsequently stained up to $5x10^6$ cells per 100µL with the following anti-human antibodies: , CD3 (BW264/56, VioBlue, Miltenyi Biotec, Cat No 130-113-133, 1:400), CD14 (TÜK4, VioBlue, Miltenyi Biotec, Cat No 130-113-152, 1:200), CD16 (REA423, VioBlue, Miltenyi Biotec, Cat No 130-113-958, 1:100), CD27 (MT271, PE, Miltenyi Biotec, Cat No 130-097-926, 1:100) and CD38 (HIT2, APC, BioLegend, Cat No 303510, 1:20). DAPI was added before sorting to allow dead cell exclusion. Activated B cells were identified and sorted as $DAPI^-CD3^-CD14^-CD16^-CD38^{high}CD27^{high}$. Alternatively, B cells were sorted from frozen PBMCs. To that end, PBMCs were stained as described but with the following anti-human antibodies: CD19 (LT19, Miltenyi Biotec, Cat No 130-113-728, 1:400), CD3 (BW264/56, VioBlue, Miltenyi Biotec, Cat No 130-113-133, 1:400), CD14 (TÜK4, VioBlue, Miltenyi Biotec, Cat No 130-113-152, 1:200), CD27 (MT271, PE, Miltenyi Biotec, Cat No 130-097-926, 1:100) and CD38 (IB6, PE-Vio770, Miltenyi Biotec, Cat No 130-113-990, 1:200). DAPI was added before sorting to allow dead cell exclusion. Activated B cells were identified and sorted as $DAPI^-CD3^-CD14^-CD19^+CD38^{high}CD27^{high}$.All sortings were preformed using a MA900 Multi-Application Cell Sorter (Sony Biotechnology). Cell counting was performed using a MACSQuant flow cytometer (Miltenyi Biotec). The sorted $CD38^{high}CD27^{high}$ cells were further processed for single cell RNA sequencing.

T cell isolation from peripheral blood and flow cytometric analysis

Isolation of SARS-CoV-2reactive effector/memory and regulatory $CD4^+$ T lymphocytes was performed as described (Okhrimenko, A, 2014, PNAS). At least $5x10^6$ PBMCs were stimulated for 6 h with anti-CD28 (1µg/mL) and the mixed spike glycoprotein (S), the membrane glycoprotein (M), and the nucleocapsid

phosphoprotein (N) of the SARS-CoV-2, each 1 µg/peptide/mL, in the presence of 1 µg/mL anti-CD40. Stimulated cells were enrichment by MACS for $CD137^+$ and $CD154^+$ cells in two consecutive MS columns (Miltenyi Biotec) and the enriched cells incubated with anti-human Cite-seq antibodies (CD154 Cat No 310849, CD127 Cat No 351356, CD45RA Cat No 310951, CD45RO Cat No 304163, CD69 Cat No 304259, CD39 Cat No 328237, HLA-DR Cat No 307663, CD279 Cat No 329963, CD57 Cat No 393321, CD27 Cat No 305651, and CD95 Cat No 302853, all from Biolegend and used according to manufacturer's instructions) for 30min. Cells were also stained for 15min with the following anti-human antibodies: CD3 (OKT3, BV785, Biolegend, Cat No 317330, 1:100), CD4 (SK3, PE-Cy5.5, Biolegend, Cat No 35-0047-42, 1:200), CD19 (H1B19, V500, BD Biosciences, Cat No 561121, 1:100), CD14 (TM1, Pacific Orange, DRFZ in-house conjugation, 1:100), CD137 (4B4-1, PE, Miltenyi Biotec, Cat No 130-093-476, 1:25) and CD154 (5C8, biotin, Miltenyi Biotec, Cat No 5190204135, 1:10). Streptavidin (eFluor450, eBioscience, Cat No 48-4317-1597, 1:200) was used subsequently. Total antigen-reactive effector/memory and regulatory $CD4^+$ T cells were identified as $PI^-CD19^-CD14^-CD3^+CD4^+$ $CD154^+$ and/or $CD137^+$ and sorted using a MA900 Multi-Application Cell Sorter (Sony Biotechnology). Cell counting was performed using a MACSQuant flow cytometer (Miltenyi Biotec). The sorted SARS-CoV-2-reactive $CD4^+$ T cells were further processed for single cell RNA sequencing. As a control measles-reactive memory $CD4^+$ T lympohocytes were also isolated and further processed for single cell sequencing. To that end, PBMCs were stimulated as described, but in presence of 5µg/mL measles lysate instead of SARS-CoV-2 proteins. Measles-reactive memory $CD4^+$ T cells were identified and sorted by the expression of $PI^-CD19^-CD14^-$ $CD3^+CD4^+CD45RO^+CD154^+$.
The phenotype of the SARS-CoV-2-stimulated cells was analyzed by flow cytometry, staining with the following anti-human antibodies: CD3 (OKT3, BV785, Biolegend Cat No 317330, 1:100), CD19 (H1B19, V500, BD Cat No 561121, 1:100), CD14 (TM1, Pacific Orange, in house conjugated, 1:100), CD4 (SK3, PE-Cy5.5, Biolegend Cat No 35-0047-42, 1:200), CD45RA (HI100, BV605, Biolegend Cat No 304133, 1:200), CCR7 (G043H7, A488, Biolegend Cat No 353206, 1:100), CD69 (FN50, PE-CF594, BD Biosciences Cat No 5049599, 1:200), HLA-DR (L243, APC-Cy7, Biolegend Cat No 307617, 1:100), CD154 (24-31, BV421, Biolegend Cat No 310824, 1:100), CD137 (4B4-1, PE, Miltenyi Biotec Cat No 130-093-476, 1:25), IFNγ (4S.B3, PE-Cy7, Biolegend Cat No 502528, 1:200), IL-2 (MQ1-17H12, APC-Cy7, Biolegend Cat No 500342, 1:100), TNFα (Mab11, APC, BD Pharminogen Cat No 554514, 1:100), and fixable Live/Dead or propidium iodide (PI). Cells were acquired using a LSRFortessa flow cytometer (BD Biosciences) with FACSDiva (BD Biosciences) software and analyzed with FlowJo (Tree Star).

Single Cell RNA-library preparation and sequencing

Single cell suspensions were obtained by cell sorting and applied to the 10x Genomics workflow for cell capturing and scRNA gene expression (GEX) and TCR/BCR/CiteSeq library preparation using the Chromium Single Cell 5' Library & Gel Bead Kit as well as the Single Cell 5' Feature Barcode Library Kit (10x Genomics). After cDNA amplification the CiteSeq libraries were prepared separately using the Single Index Kit N Set A. TCR/BCR target enrichment was performed using the Chromium Single Cell V(D)J Enrichment Kit for Human T cells and B cells respectively. Final GEX and TCR/BCR libraries were obtained after fragmentation, adapter ligation and final Index PCR using the Single Index Kit T Set A. Qubit HS DNA assay kit (life technologies) was used for library quantification and fragment

sizes were determined using the Fragment Analyzer with the HS NGS Fragment Kit (1-6000bp) (Agilent).
Sequencing was performed on a NextSeq500 device (Illumina) using High Output v2 Kits (150 cycles) with the recommended sequencing conditions for 5' GEX libraries (read1: 26nt, read2: 98nt, index1: 8nt, index2: n.a.) and Mid Output v2 Kits (300 cycles) for TCR/BCR libraries (read1: 150nt, read2: 150nt, index1: 8nt, index2: n.a., 20% PhiX spike-in).

Single-cell transcriptome Sequencing, and BCR and TCR repertoire profiling
Raw sequence reads were processed using cellranger-3.1.0, including the default detection of intact cells. Mkfastq, count and vdj were used in default parameter settings for demultiplexing, quantifying the gene expression and assembly of the B cell and T cell receptor sequences. Refdata-cellranger-hg19-1.2.0 and refdata-cellranger-vdj-GRCh38-alts-ensembl-2.0.0 were used as reference. The number of expected cells was set to 3000. Data from transcriptome sequencing and immune profiling in GEO under the accession GSEXXXXX.
The cellranger output was further analyzed in R using the Seurat package (version 3.1.1)(Butler et al., 2018). In particular, transcriptome profiles for 13 COVID patients and 5 healthy controls were merged, normalized, variable genes were detected and a Uniform Manifold Approximation and Projection (UMAP) was performed in default parameter settings using FindVariableGenes, RunPCA and RunUMAP with 30 principle components. Expression values are represented as ln (10,000 * UMIsGene) /UMIsTotal +1). Transcriptionally similar clusters were identified using shared nearest neighbor (SNN) modularity optimization, SNN resolutions ranging from 0.1 to 1.0 in 0.1 increments were computed, or gating was performed manually using the Loupe Browser (10x Genomics). Subsequently, clusters were annotated by projection of *CD19*, *MS4A1*, *CD27*, *CD38*, *IFIT1*, *MIKI67*, *IRF4* and *PRDM1* expression on the UMAP to assign different activation/proliferation/differentiation stages of B cell and signature genes were identified using FindAllMarkers in default parameter settings. Heatmaps are based on z-transformed expression values for genes with significant differences to means in different clusters as judged by a Bonferroni corrected P-Value (Wilcoxon rank sum Test) below 0.01 and an minimal absolute fold-change to the mean of log2(1.3).
Data from transcriptome and immune profiling were merged by the same cellular barcodes. The high-confidence contig sequences for barcodes with known transcriptional profile were reanalyzed using HighV-QUEST at IMGT web portal for immunoglobulin (IMGT) to retrieve the V-, J- and D-genes as nucleotide and amino acid CDR3 sequence. IMGT-gapped-nt-sequences, V-REGION-mutation-and-AA-change-table as well as nt-mutation-statistics were used to determine the corresponding gapped germline FR1, CDR1, FR2, CDR2, FR3 sequences as well as estimated mutation counts in the FR1-FR3 region. The most abundant contig for the heavy and light BCR chain was assigned to the corresponding cell in the single cell transcriptome analysis. Cells with incomplete heavy and light chain annotation were removed from further analysis. This led to the annotation of 6258, 2678, 2437, 7480, 4704, 7527, 4922, 4743, and 9168 transcriptome profiles for 9 COVID Patients and 1571, 1621 and 2633 for three healthy donors. In case of two contigs for the heavy chain the alternative contig was defined as the inactive heavy chain gene locus transcript, if found nonproductive. For the hypermutation analysis clonal families were defined by the same VJ-gene usage, gapped germline FR1-FR3 sequence and the nucleotide CDR3 sequence length of the heavy and light chain. The hypermutation trees were computed using GLaMST with concatenated FR1-FR3 sequences of the

heavy and light chain and the germline sequence as root input. The effective diversity for different Hill orders were computed based on the FR1-FR3 germline sequence, used vj-gene and the cdr3nt sequence. The same procedure was used for the analysis of time changes between different time points for patients #1 and #9. The first samples at day 4 and day 31 were reanalyzed with the corresponding samples at day 59 and day 46 for patient #1 and patient #9, respectively. For the overlaps between bronchoalveolar lavage (BAL) and peripheral blood sample of patient #1, a separated immune profile was used.
For TCR analysis samples from 3 COVID-19 patients and 2 healthy control were tagged with citeseq antibodies, pooled, sequenced and analyzed in analogy to the B cells. Transcriptome and immune profiles were merged by same barcodes. For the V, D and J, the CDR3nt, CDR3aa and Isotype were directly taken from the cellranger results. In case of more than one contig for the heavy or light TCR chain the most abundant, productive contig was chosen. Different sample origin was demultiplexed using sample specific hash code.

Gene Set Enrichment Analysis (GSEA)
The IL2/IL21 signature of activated B cells and additional subsequent treatment with IL6/IL21/IFN I, IL6/IL21/TGF-β and IL6/IL21/IFN I/TGF-β was derived from a publication of Stephenson and colleagues(Stephenson et al., 2019). Quantile normalized Illumina HumanHT-12 beadchip expression values for Il2/IL21-activated B cells with and without additional treatment was obtained from GEO (accession number GSE120367). Sparse Partial Least Squares Discriminant Analysis (sPLS-DA) was performed using mixOmics R-package by keeping 200 genes in 3 components. Expression values from Stephenson *et al*. and the 10xGenomics data from this study was based on gene symbols. Solely genes with non-redundant symbols and unique equivalent in 10x genomics sequencing were used. sPLS-DA was performed separately for 12h, 24h and 48h after stimulation. IL2/IL21-activated B cells at day 6 were used as control (Supplementary Methods Fig 1.). *TGFB*-Signature genes were defined by positive loadings on component 2. Signature genes were defined by negative contribution to Component 1 for IL2/IL21-activated B cell signature, negative contribution to Component 2 for IL6/IL21/IFN I treatment, positive contribution to Component 3 for and IL6/IL21/IFN I/TGF-β treatment and positive contribution to Component 2 for and IL6/IL21/TGF-β.
GSEA was performed for each cell, using the natural logarithm of the fold change expression relative to mean expression of all cell as pre ranked list and 1000 randomizations. Statistically significant up- or downregulation was defined by a FDR ≤ 0.25 and normalize p value < 0.05 (Subramanian et al., 2005). For visualization NES for significant cells were plotted.

Flow cytometric analysis of anti-spike protein serum antibody titers
HEK293T cells were transfected with a plasmid expressing wild-type SARS-CoV-2 S protein(Hoffmann et al., 2020). Next day, transfected cells were collected and incubated with sera or recombinant anti-SARS-CoV-2 Spike Glycoprotein S1 antibody [CR3022] (ab273073; Abcam) for 30 min, washed twice with PBS/BSA and stained with anti-human IgG-Alexa647 (Southern Biotech), PE anti-IgM (Biolegend) and FITC anti-IgA (Southern Biotech), anti-human IgA1 Alexa488 (Southern Biotech), anti-human IgA2-Alexa647 (Southern Biotech) for 30 min. Cells were washed with PBS/BSA and DAPI was added before analysis for dead cell exclusion. Samples were analyzed on a FACSCanto (BD Biosciences) and using FlowJo v10 (Tree Star Inc.) analysis software. Mean fluorescent intensities were determined for transfected

and non-transfected cells of each sample. Data were presented as ΔMFI=MFI(transfected)-MFI(non-transfected).

ELISA analysis of anti-spike protein, its RBD domain and anti-nucleoprotein serum antibody titers

Antibody titers against various Sars-Cov-2 S protein were measured using COVID-19 Human IgM IgG Assay Kit (Abnova, Cat No ABN-KA5826) with slight modifications: anti-S IgG and IgM were quantified according to manufacturer's instructions. To analyse S protein specific IgA1 and IgA2 responses, detection was performed using mouse anti-human IgA1-AP (Southern Biotech) and anti-human IgA2-AP (Southern Biotech), followed by pNPP substrate. Quantification of anti-S-RBD and anti-NP Sars-CoV-2 antibody responses has been performed using respective recombinant proteins. Briefly, plates were coated with 100 µL PBS containing 1µg/ml of Spike RBD-His Recombinant Protein (Sino Biological) or SARS-CoV-2 Nucleocapsid His Protein (RnD systems) overnight at 4°C. Plates were blocked with 5% PBS/BSA for one hour, serial dilution of sera were applied and incubated overnight at 4°C. Antibodies were detected using anti-human IgG (MP biomedicals), IgM (Sigma-Aldrich), IgA1 (Southern Biotech) and IgA2 (Southern Biotech) coupled with alkaline phosphatase, followed by pNPP substrate. Reactions were stopped by adding NaOH and absorbance values at 405nm were measured using SpectraMax plate reader (Molecular devices). Antibody titers were quantified using non-linear curve fit in GraphpadPrism 5.0. Spearman rank correlation was applied for analysis of correlations between ELISA- and flow cytometry- based antibody measurements.

SARS-CoV-2 neutralization assay

Pseudovirus neutralization assay for SARS-CoV-2 was preformed as previously described(Nie et al., 2020; Tan et al., 2020). Briefly, 2µL of serum or serum dilutions were pre-incubated for 1 hour at 37°C with 10µL of virus in 10µL PBS. The pre-incubated serum/virus suspensions were then added to VeroE6 cells cultured in 100µL DMEM 5% hiFCS on a 96-well plate, and incubated at 37°C for 1 day before readout (plaques/Fluorescent foci). Assay was performed in duplicate wells, three dilutions per serum. Analysis was done using averages of 4 fields of view chosen randomly (blind) and then assessed for foci using fluorescent microscopes.

Antibody generation

From the VH and VL sequences obtained by scRNA, synthetic GeneBlocks were synthesized (IDTDNA, Leuwen, Belgium) and cloned into expression vectors for human IgG1 and human Igk, essentially as described by Tiller et al. (Tiller et al., 2008), except that we used Gibson assembly for the cloning. Heavy and light chain plasmids were transfected into 293 freestyle cells as recommended by the manufacturer and antibodies were purified on a Protein G column from the culture supernatants.

Cytokine measurements

Blood plasma was diluted 1:3, and IL-21, IFN-α, and IFN-y were detected using a bead-based multiplex cytokine array (ProcartaPlex Human Cytokine Panel 1B, Thermo Fisher Scientific). TGF-β was detected using the ProcartaPlex Human TGF-beta 1 Simplex Kit (Thermo Fisher Scientific). Prior to measuring plasma-TGF-β1, the bioactive form of TGF-β1 was generated by incubating the plasma with 1 N HCl followed by neutralization with 1.2N NaOH according to the manufacturer's

instructions. All cytokines were measured using the Luminex MAGPIX instrument and quantified using the xPONENT analysis software (Luminex Corporation).

Tissue preparation for MELC

Fresh frozen lungs tissue was cut into 5 µm sections with a NX80 cryotome (ThermoFisher, Waltham, Massachusetts, USA), and deposited on APES-coated cover slides (24 x 60 mm; Menzel-Gläser, Braunschweig, Germany). Samples were fixed for 10 minutes at RT with 2% paraformaldehyde (methanol- and RNAse-free; Electron Microscopy Sciences, Hatfield, Philadelphia, USA). After washing samples were permeabilized with 0.2% Triton X-100 in PBS for 10 min at room temperature and blocked with 10% goat serum and 1% BSA in PBS for at least 20 minutes. Afterwards, a fluid chamber holding 100 µl of PBS was created using “press-to-seal” silicone sheets (Life technologies, Carlsbad, California, USA; 1.0 mm thickness), which were attached to the cover slip, surrounding the sample.

MELC Image Acquisition

We generated the multiplexed histology data on a modified Toponome Image Cycler® MM3 (TIC) originally produced by MelTec GmbH & Co.KG Magdeburg, Germany (Holzwarth et al., 2018; Schubert et al., 2006). The robotic microscopic system consists of: (i) an inverted widefield (epi)fluorescence microscope Leica DM IRE2 equipped with a CMOS camera and a motor-controlled XY-stage, (ii) CAVRO XL3000 Pipette/Diluter (Tecan GmbH, Crailsheim, Germany), and (iii) a software MelTec TIC-Control for controlling microscope and pipetting system and for synchronized image acquisition. The MELC run is a sequence of cycles, each containing the following four steps: (i) incubation of the fluorescence-coupled antibody and subsequent washing; (ii) cross-correlation based auto-focusing; (iii) photo-bleaching of the fluorophore; and (iv) a second autofocusing step followed by acquisition of a 3D stack post-bleaching fluorescence image. In each four-step cycle another fluorescence-labeled antibody is used. After the sample was labeled sequentially by DAPI (Roche, Cat. No. 10236276001, dilution 1:5000) and all antibodies of interest as described above, the experiment was completed. Fluorescence-coupled antibodies used: IgA2-PE (Clone REA995, Miltenyi, Cat. No.130-117-763, dilution 1:50); CD27-PE (Clone REA499, Miltenyi, Cat. No. 130-114-166, dilution 1:50); CD38-PE (Clone IB6, Miltenyi, Cat. No. 130-113-427, dilution 1:50) and IgA-PE (Clone IS11-8E10, Miltenyi, Cat. No. 130-114-002, dilution 1:50). The antibodies were stained in the indicated order.

Image pre-processing

In short, all images were aligned based on the reference phase contrast image taken at the beginning of the measurement. Afterwards, each fluorescence MELC image was processed by background subtraction and illumination correction, based on the bleaching images(Schubert et al., 2006). In order to account for slice thickness, an “Extended Depth of Field” algorithm was applied on the 3D fluorescence stack in each cycle(Pertuz et al., 2013). Images were then normalized in ImageJ(Abramoff et al., 2004), where a rolling ball algorithm was used for background estimation, edges were removed (accounting for the maximum allowed shift during the autofocus procedure) and fluorescence intensities were stretched to the full intensity range (16 bit -> 2^{16}).

Autopsy tissue

Autopsies were performed at the Department of Pathology and Neuropathology, Charité - Universitätsmedizin Berlin. For sampling postmortem tissue from COVID-19 and control patients, its virological assessment and the histological analysis, the approval from the Ethics Committee of the Charité included EA 1/144/13 with EA 1/075/19 and EA2/066/20 Substudy No.60. The study was in compliance with the Declaration of Helsinki. In all included deceased patients a whole-body autopsy was performed, which included a thorough histopathologic and molecular evaluation comprising virological assessment of SARS-CoV-2 RNA levels as previously described(Corman et al., 2020). Clinical records were assessed for pre-existing medical conditions and medications, current medical course, and ante-mortem diagnostic findings as specified in supplementary Fig. 4a. Cause of death for the control cases was aspiration pneumonia and COVID-19 for the SARS-CoV-2 infected patients.

Acknowledgements

We thank Jenny Kirsch, Ana Catalina Teichmüller and Toralf Kaiser for support in cell sorting. We are indebted to Francisca Egelhofer and Anistan Sebastiampillai for excellent technical assistance and advice. The authors are most grateful to the patients and their relatives for consenting to autopsy and subsequent research, which were done with support of the BrainBank of the Department of Neuropathology – Universitätsmedizin Berlin, Germany. This Work was supported by the state of Berlin and the “European Regional Development Fund” to M.F.M. (ERDF 2014–2020, EFRE 1.8/11, Deutsches Rheuma-Forschungszentrum), the Berlin Institute of Health with the Starting Grant - Multi-Omics Characterization of SARS-CoV-2 infection, Project 6 ”Identifying immunological targets in Covid-19” to H.D.V., A.D. and M.F.M., by the Deutsche Forschungsgemeinschaft through the TRR130-P16 and P17 to A.R., H.D.C. and H.R., by the European Research Council through the Advanced Grant IMMEMO (ERC-2010-AdG.20100317 Grant 268978) to A.R., and by the DFG– Projektnummer 389687267 to J.D. and A.R.. A.K. was supported by DFG (TRR241 A04), Russian Science Foundation grant (# 17-74-20059; measurement of serum IgA responses) and Russian fund for basic research (#17-00-00435). A.E.H. was funded by the DFG (TRR130-C01 and P17, HA5354/6-2 and HA5354/8-2). L.B., J.N. and H.D.C. were funded by the Dr. Rolf M. Schwiete Foundation.

Contributions

Conceptualization: M.F.M., A.R., F.M.; Methodology: M.F.G., A.K, P.D, G.A.H., A.P.R., W.D., S.F. K.H.; Software: F.H., P.D.; Validation: M.F.M., M.F.G., A.K., C.T., G.A.H.; Formal analysis: F.H., P.D.; Investigation: M.F.G., A.K., C.T., G.A.H., A.P.R., W.D., R.M., C.F., S.F., K.H. L.B., J.N., P.K.J., G.M.G, K.L., L.O., L.H., S.B. Resources: G.S., M.R., T.K, M.A.M, S.A., S.T., V.M.C, S.E., H.R., M.W; Data curation: M.F.M., F.H., P.D.; Writing - original draft: A.R., F.M., M.F.M., and M.F.G.; Writing - Review & editing: M.F.G., G.A.H.; Visualization: F.H., P.D., A.K., M.F.M, A.P.R; Supervision: H.D.C.,T.D., A.D., M.M., H.D.V., T.H.W., J.D., A.E.H., H.R., M.W., F.M., A.R., M.F.M; Project administration: M.F.M., A.R., F.M.; Funding acquisition: A.R., M.F.M.

References

Abramoff, M.D., Magalhães, P.J., and Ram, S.J. (2004). Image processing with ImageJ. Biophotonics international *11*, 36-42.

Bacher, P., Heinrich, F., Stervbo, U., Nienen, M., Vahldieck, M., Iwert, C., Vogt, K., Kollet, J., Babel, N., Sawitzki, B.*, et al.* (2016). Regulatory T Cell Specificity Directs Tolerance versus Allergy against Aeroantigens in Humans. Cell *167*, 1067-1078 e1016.
Becht, E., McInnes, L., Healy, J., Dutertre, C.A., Kwok, I.W.H., Ng, L.G., Ginhoux, F., and Newell, E.W. (2018). Dimensionality reduction for visualizing single-cell data using UMAP. Nat Biotechnol.
Butler, A., Hoffman, P., Smibert, P., Papalexi, E., and Satija, R. (2018). Integrating single-cell transcriptomic data across different conditions, technologies, and species. Nat Biotechnol *36*, 411-420.
Chu, H.W., Trudeau, J.B., Balzar, S., and Wenzel, S.E. (2000). Peripheral blood and airway tissue expression of transforming growth factor beta by neutrophils in asthmatic subjects and normal control subjects. J Allergy Clin Immunol *106*, 1115-1123.
Corman, V.M., Landt, O., Kaiser, M., Molenkamp, R., Meijer, A., Chu, D.K., Bleicker, T., Brunink, S., Schneider, J., Schmidt, M.L.*, et al.* (2020). Detection of 2019 novel coronavirus (2019-nCoV) by real-time RT-PCR. Euro Surveill *25*.
Cyster, J.G., and Allen, C.D.C. (2019). B Cell Responses: Cell Interaction Dynamics and Decisions. Cell *177*, 524-540.
Fensterl, V., and Sen, G.C. (2015). Interferon-induced Ifit proteins: their role in viral pathogenesis. J Virol *89*, 2462-2468.
Fujieda, S., Saxon, A., and Zhang, K. (1996). Direct evidence that gamma 1 and gamma 3 switching in human B cells is interleukin-10 dependent. Mol Immunol *33*, 1335-1343.
Grifoni, A., Sidney, J., Zhang, Y., Scheuermann, R.H., Peters, B., and Sette, A. (2020). A Sequence Homology and Bioinformatic Approach Can Predict Candidate Targets for Immune Responses to SARS-CoV-2. Cell Host Microbe *27*, 671-680 e672.
Gutcher, I., Donkor, M.K., Ma, Q., Rudensky, A.Y., Flavell, R.A., and Li, M.O. (2011). Autocrine transforming growth factor-beta1 promotes in vivo Th17 cell differentiation. Immunity *34*, 396-408.
Hall, M.C., Young, D.A., Waters, J.G., Rowan, A.D., Chantry, A., Edwards, D.R., and Clark, I.M. (2003). The comparative role of activator protein 1 and Smad factors in the regulation of Timp-1 and MMP-1 gene expression by transforming growth factor-beta 1. J Biol Chem *278*, 10304-10313.
He, L., Ding, Y., Zhang, Q., Che, X., He, Y., Shen, H., Wang, H., Li, Z., Zhao, L., Geng, J.*, et al.* (2006). Expression of elevated levels of pro-inflammatory cytokines in SARS-CoV-infected ACE2+ cells in SARS patients: relation to the acute lung injury and pathogenesis of SARS. J Pathol *210*, 288-297.
Hoffmann, M., Kleine-Weber, H., Schroeder, S., Kruger, N., Herrler, T., Erichsen, S., Schiergens, T.S., Herrler, G., Wu, N.H., Nitsche, A.*, et al.* (2020). SARS-CoV-2 Cell Entry Depends on ACE2 and TMPRSS2 and Is Blocked by a Clinically Proven Protease Inhibitor. Cell *181*, 271-280 e278.
Holzwarth, K., Kohler, R., Philipsen, L., Tokoyoda, K., Ladyhina, V., Wahlby, C., Niesner, R.A., and Hauser, A.E. (2018). Multiplexed fluorescence microscopy reveals heterogeneity among stromal cells in mouse bone marrow sections. Cytometry A *93*, 876-888.
Islam, K.B., Nilsson, L., Sideras, P., Hammarstrom, L., and Smith, C.I. (1991). TGF-beta 1 induces germ-line transcripts of both IgA subclasses in human B lymphocytes. Int Immunol *3*, 1099-1106.
Itoh, Y., Saitoh, M., and Miyazawa, K. (2018). Smad3-STAT3 crosstalk in pathophysiological contexts. Acta Biochim Biophys Sin (Shanghai) *50*, 82-90.

Johansen, F.E., Braathen, R., and Brandtzaeg, P. (2000). Role of J chain in secretory immunoglobulin formation. Scand J Immunol *52*, 240-248.
Jung, S., Rajewsky, K., and Radbruch, A. (1993). Shutdown of class switch recombination by deletion of a switch region control element. Science *259*, 984-987.
Kee, B.L., Rivera, R.R., and Murre, C. (2001). Id3 inhibits B lymphocyte progenitor growth and survival in response to TGF-beta. Nat Immunol *2*, 242-247.
Kitani, A., and Strober, W. (1993). Regulation of C gamma subclass germ-line transcripts in human peripheral blood B cells. J Immunol *151*, 3478-3488.
Kwon, H., Thierry-Mieg, D., Thierry-Mieg, J., Kim, H.P., Oh, J., Tunyaplin, C., Carotta, S., Donovan, C.E., Goldman, M.L., Tailor, P.*, et al.* (2009). Analysis of interleukin-21-induced Prdm1 gene regulation reveals functional cooperation of STAT3 and IRF4 transcription factors. Immunity *31*, 941-952.
Lee, Y., Awasthi, A., Yosef, N., Quintana, F.J., Xiao, S., Peters, A., Wu, C., Kleinewietfeld, M., Kunder, S., Hafler, D.A.*, et al.* (2012). Induction and molecular signature of pathogenic TH17 cells. Nat Immunol *13*, 991-999.
Lorenz, M., Jung, S., and Radbruch, A. (1995). Switch transcripts in immunoglobulin class switching. Science *267*, 1825-1828.
Mei, H.E., Frolich, D., Giesecke, C., Loddenkemper, C., Reiter, K., Schmidt, S., Feist, E., Daridon, C., Tony, H.P., Radbruch, A.*, et al.* (2010). Steady-state generation of mucosal IgA+ plasmablasts is not abrogated by B-cell depletion therapy with rituximab. Blood *116*, 5181-5190.
Mellado, M., Rodriguez-Frade, J.M., Aragay, A., del Real, G., Martin, A.M., Vila-Coro, A.J., Serrano, A., Mayor, F., Jr., and Martinez, A.C. (1998). The chemokine monocyte chemotactic protein 1 triggers Janus kinase 2 activation and tyrosine phosphorylation of the CCR2B receptor. J Immunol *161*, 805-813.
Mokrani, M., Klibi, J., Bluteau, D., Bismuth, G., and Mami-Chouaib, F. (2014). Smad and NFAT pathways cooperate to induce CD103 expression in human CD8 T lymphocytes. J Immunol *192*, 2471-2479.
Nie, J., Li, Q., Wu, J., Zhao, C., Hao, H., Liu, H., Zhang, L., Nie, L., Qin, H., Wang, M.*, et al.* (2020). Establishment and validation of a pseudovirus neutralization assay for SARS-CoV-2. Emerg Microbes Infect *9*, 680-686.
Odendahl, M., Mei, H., Hoyer, B.F., Jacobi, A.M., Hansen, A., Muehlinghaus, G., Berek, C., Hiepe, F., Manz, R., Radbruch, A.*, et al.* (2005). Generation of migratory antigen-specific plasma blasts and mobilization of resident plasma cells in a secondary immune response. Blood *105*, 1614-1621.
Parrish-Novak, J., Dillon, S.R., Nelson, A., Hammond, A., Sprecher, C., Gross, J.A., Johnston, J., Madden, K., Xu, W., West, J.*, et al.* (2000). Interleukin 21 and its receptor are involved in NK cell expansion and regulation of lymphocyte function. Nature *408*, 57-63.
Pene, J., Gauchat, J.F., Lecart, S., Drouet, E., Guglielmi, P., Boulay, V., Delwail, A., Foster, D., Lecron, J.C., and Yssel, H. (2004). Cutting edge: IL-21 is a switch factor for the production of IgG1 and IgG3 by human B cells. J Immunol *172*, 5154-5157.
Pertuz, S., Puig, D., Garcia, M.A., and Fusiello, A. (2013). Generation of all-in-focus images by noise-robust selective fusion of limited depth-of-field images. IEEE Trans Image Process *22*, 1242-1251.
Polak, S.B., Van Gool, I.C., Cohen, D., von der Thusen, J.H., and van Paassen, J. (2020). A systematic review of pathological findings in COVID-19: a pathophysiological timeline and possible mechanisms of disease progression. Mod Pathol.

Radbruch, A., Burger, C., Klein, S., and Muller, W. (1986). Control of immunoglobulin class switch recombination. Immunol Rev *89*, 69-83.
Riedel, R., Addo, R., Ferreira-Gomes, M., Heinz, G.A., Heinrich, F., Kummer, J., Greiff, V., Schulz, D., Klaeden, C., Cornelis, R.*, et al.* (2020). Discrete populations of isotype-switched memory B lymphocytes are maintained in murine spleen and bone marrow. Nat Commun *11*, 2570.
Schubert, W., Bonnekoh, B., Pommer, A.J., Philipsen, L., Bockelmann, R., Malykh, Y., Gollnick, H., Friedenberger, M., Bode, M., and Dress, A.W. (2006). Analyzing proteome topology and function by automated multidimensional fluorescence microscopy. Nat Biotechnol *24*, 1270-1278.
Sciammas, R., Shaffer, A.L., Schatz, J.H., Zhao, H., Staudt, L.M., and Singh, H. (2006). Graded expression of interferon regulatory factor-4 coordinates isotype switching with plasma cell differentiation. Immunity *25*, 225-236.
Shaim, H., Estrov, Z., Harris, D., Hernandez Sanabria, M., Liu, Z., Ruvolo, P., Thompson, P.A., Ferrajoli, A., Daher, M., Burger, J.*, et al.* (2017). The CXCR4-STAT3-IL-10 Pathway Controls the Immunoregulatory Function of Chronic Lymphocytic Leukemia and Is Modulated by Lenalidomide. Front Immunol *8*, 1773.
Stein, J.V., and Nombela-Arrieta, C. (2005). Chemokine control of lymphocyte trafficking: a general overview. Immunology *116*, 1-12.
Stephenson, S., Care, M.A., Fan, I., Zougman, A., Westhead, D.R., Doody, G.M., and Tooze, R.M. (2019). Growth Factor-like Gene Regulation Is Separable from Survival and Maturation in Antibody-Secreting Cells. J Immunol *202*, 1287-1300.
Subramanian, A., Tamayo, P., Mootha, V.K., Mukherjee, S., Ebert, B.L., Gillette, M.A., Paulovich, A., Pomeroy, S.L., Golub, T.R., Lander, E.S.*, et al.* (2005). Gene set enrichment analysis: a knowledge-based approach for interpreting genome-wide expression profiles. Proc Natl Acad Sci U S A *102*, 15545-15550.
Tan, C.W., Chia, W.N., Qin, X., Liu, P., Chen, M.I., Tiu, C., Hu, Z., Chen, V.C., Young, B.E., Sia, W.R.*, et al.* (2020). A SARS-CoV-2 surrogate virus neutralization test based on antibody-mediated blockage of ACE2-spike protein-protein interaction. Nat Biotechnol.
Tiller, T., Meffre, E., Yurasov, S., Tsuiji, M., Nussenzweig, M.C., and Wardemann, H. (2008). Efficient generation of monoclonal antibodies from single human B cells by single cell RT-PCR and expression vector cloning. J Immunol Methods *329*, 112-124.
Tomcik, M., Palumbo-Zerr, K., Zerr, P., Avouac, J., Dees, C., Sumova, B., Distler, A., Beyer, C., Cerezo, L.A., Becvar, R.*, et al.* (2015). S100A4 amplifies TGF-beta-induced fibroblast activation in systemic sclerosis. Ann Rheum Dis *74*, 1748-1755.
Van Obberghen-Schilling, E., Roche, N.S., Flanders, K.C., Sporn, M.B., and Roberts, A.B. (1988). Transforming growth factor beta 1 positively regulates its own expression in normal and transformed cells. J Biol Chem *263*, 7741-7746.
Vu Van, D., Beier, K.C., Pietzke, L.J., Al Baz, M.S., Feist, R.K., Gurka, S., Hamelmann, E., Kroczek, R.A., and Hutloff, A. (2016). Local T/B cooperation in inflamed tissues is supported by T follicular helper-like cells. Nat Commun *7*, 10875.
Wiesner, B., Bachmann, M., Blum, T.G., Forchheim, S., Geiseler, J., Kassin, A., Kretzschmar, E., Weber-Carstens, S., Westhoff, M., Witzenrath, M.*, et al.* (2020). [Responsibilities of Weaning Centers during the COVID-19 Pandemic Outbreak - Recommendations for the Assignment of ICU Capacities in COVID-19 Patients as shown by the Berlin-Brandenburg POST-SAVE-Model]. Pneumologie *74*, 358-365.
Wrammert, J., Koutsonanos, D., Li, G.M., Edupuganti, S., Sui, J., Morrissey, M., McCausland, M., Skountzou, I., Hornig, M., Lipkin, W.I.*, et al.* (2011). Broadly cross-reactive antibodies

dominate the human B cell response against 2009 pandemic H1N1 influenza virus infection. J Exp Med *208*, 181-193.
Zhao, X., Nicholls, J.M., and Chen, Y.G. (2008). Severe acute respiratory syndrome-associated coronavirus nucleocapsid protein interacts with Smad3 and modulates transforming growth factor-beta signaling. J Biol Chem *283*, 3272-3280.

Figure Legends

Figure 1. Single cell transcriptomes of COVID-19 patients show dynamic differences of activated B cell subpopulations at different stages after ICU admission. Peripheral blood activated B cells ($CD27^{high}$ $CD38^{high}$) were isolated and sorted by FACS for single cell sequencing. **a)** Percentage of $CD27^{high}$ $CD38^{high}$ cells among live B cells. Each sample is represented by a circle. The line indicates the median. Unpaired two sided Mann-Whitney U test. **b)** UMAP representation of 72277 $CD27^{high}$ $CD38^{high}$ sorted B cells from 9 COVID-19 ICU patients and 3 healthy controls. Between 2416 and 11229 cells were recovered per sample. Transcriptionally similar clusters were identified using shared nearest neighbor (SNN) modularity optimization (left). The combination of *CD19*, *MS4A1*, *CD27*, *CD38*, *IFIT1*, *MIKI67*, *IRF4* and *PRDM1* expression were used for annotation of the different activation/differentiation stages (right). **c)** Heatmap of genes that resemble markers for the six different clusters. Depicted are genes with a p-value <0.01 (Wilcoxon rank sum test) after bonferroni correction, and an average absolute fold-change > log2(1.3). Shown are z-scores of the average expression. **d)** UMAP representation of the expression levels of selected signature genes for activated/differentiated B cells. **e)** UMAP representation of analyzed cells from one healthy control and two ICU patients, representing early (first week, patient #1) and late (>7days, patient #5) phase after ICU admission. **f)** Percentage of cells belonging to a defined cluster among all sequenced B cells per donor. Each dot represents one time point from one single donor. Donors were grouped as “HC” for healthy controls (n=3), “1st week” for patients within 7 days after ICU admission (n=6) and “Late” for patients who have been admitted to the ICU for more than a week at the time of analysis (n=8). The line indicates the median. Significance was determined by using a two-sided analysis of varience (ANOVA) folowed by Tukey’s multiple comparison test with corrected p values as indicated in the figure.

Figure 2. Peripheral activated B cells of COVID-19 patients switch their isotype and change their transcriptional signature in response to IL-21 and TGF-β in a kinetic fashion. a) Binding of IgG, IgM, IgA1 and IgA2 antibodies to SARS-Cov-2-S protein expressed on the surface of transfected 293T cells. Data represent ΔMFI, which was calculated as following: MFI of transfected cells, incubated with sera and stained with respective anti-hIg, minus MFI of untransfected cells, incubated with sera and stained with respective anti-hIg. Dotted line indicates a ΔMFI of 1500. **b)** Percentage of isotype-positive cells among sequenced $CD27^{high}$ $CD38^{high}$ B cells

determined by single cell BCR sequencing. Donors were grouped as “HC” for healthy controls (n=3), “1st week” for patients within 7 days after ICU admission (n=6) and “Late” for patients who have been admitted to the ICU for more than a week at the time of analysis (n=8). Lines indicate measurements from the same patient at different time points. Two sided Mann-Whitney U test. **c)** UMAP representation of immunoglobulin isotype expression. Percentages refer to the total number of sequenced cells per donor. For IgG1 and IgA2 of COVID-19 patients the absolute number of cells is shown. Arrows represent the time (5-31 days and see supplementary Fig. 1a) patients had spent in the ICU at the time of analysis (upper) and the shift in cytokine milieu to allow switching to IgG1/IgA1/IgA2 (left). **d)** Concentration of total IgA in the serum of COVID-19 patients at both early (less than a week) and late time points after ICU admission as determined by ELISA. Lines indicate measurements from the same patient at different time points. Wilcoxon exact test. **e)** Gene Set Enrichment Analysis (GSEA) for the IL-6/IL-21/TGF-β signature as defined by contrasting IL-2/IL-21-activated B cells and IL-2/IL-21-activated B cells with an additional IL-6/IL-21/type I IFN, IL-6/IL-21/TGF-β or IL-6/IL-21/type I IFN/TGF-β treatment for 12h, 24h and 48h (stimulation data by Stephen *et al.*(Stephenson et al., 2019)). GSEA was performed for each cell relative to the mean expression in COVID-19 and healthy control samples. Cells were colored by the normalized enrichment score (NES) if statistically significant, with red and blue color shades for up- and down-regulation. Shown numbers refer to the number of cells showing significant up-regulation of the gene set. Arrows represent the time (5-31 days and see supplementary Fig. 1a) patients had spent in the ICU at the time of analysis (upper) and the time B cells were stimulated to generate the data sets used (left). **f)** Quantification of IFN-γ and TGF-β1 in the plasma of COVID-19 patients by cytokine bead arrays at several time points following ICU admission. Cytokine concentration in healthy individuals: IFN-γ, 63pg/mL±16pg/mL; TGF-β1, 141 pg/mL±74pg/mL.

Figure 3. SARS-CoV-2-reactive, antigen-experienced $CD4^+$ T lymphocytes are in the circulation of COVID-19 ICU patients and express IL-21 and/or TFG-β. a) Titration of SARS-Cov-2-S protein-specific IgG, IgA and IgM antibodies in the serum of 3 COVID-19 ICU patients. ΔMFI calculation as described in Fig. 2a. Dotted line indicates a ΔMFI of 1500. **b)** Workflow for the isolation and analysis of SARS-CoV-2- and measles-reactive $CD4^+$ T lymphocytes. **c)** Cells for single cell sequencing were sorted using FACS as $PI^-CD19^-CD14^-CD3^+CD4^+$ $CD154^+$ or $CD137^+$ (gating strategy as used for the analysis shown in supplementary Fig. 3b)**.** UMAP representation of 3727 $CD4^+$ T cells from 3 COVID-19 ICU patients and 2 healthy controls (SARS-CoV-2-stimulated cells from one control and measles-stimulated cells from another control). Four clusters were identified based on transcriptional similarity using shared nearest neighbor (SNN) modularity optimization (left). An additional $CD14^+$ cluster (124 cells) and 6 outlying T cells with considerably less UMI-counts than the average were also identified but excluded from further analysis. Heatmap of signature genes of the four clusters. Depicted are genes with an absolute log2 fold change > log2(2) and a p-value < 0.01 after bonferroni correction (Wilcoxon rang sum test). Colors corresponds to z-scores of the average expression. **d)** Expression levels of selected signature genes and cytokines. **e)** Expression levels of *IL21* and *TGFB1* (top, color scale). *IL21* single producers, *TGFB1* single producers, and *IL21/TGFB1* double producers among all sequenced cells, indicated for the individual donors (bottom, grey scale).The percentage of producer cells among total cells per donor is indicated in each UMAP.

Figure 4. Absence of IgA-expressing activated B cells and/or plasma cells from the lungs of severe and deceased COVID-19 patients. a) 5-marker MELC panel of SARS-CoV2-positive and control lungs (SARS-CoV2-negative). Respective patient characteristics are given in supplementary Fig. 4a. Each image of each patient depicts the same field of view of the same section, sequentially stained with the fluorescence-labelled antibodies indicated and the nuclear stain DAPI. Magenta arrows indicate $IgA2^+IgA^+CD27^+CD38^+$ cells (containing a nucleus). Images contain 2048 x 2048 pixels and are generated using an inverted wide-field fluorescence microscope with a 20x objective, a lateral resolution of 325 nm and an axial resolution above 5 µm. Scale bar: 100 µm. **b)** Absolute numbers of $IgA2^+IgA^+CD27^+CD38^+$ cells per field of view in all MELC runs acquired (two runs per patient except for COVID-19_A with four runs and Control_B with one single run; see Fig. 4a and supplementary Fig. 4b). Each field of view is represented by a circle. The line indicates the median. Unpaired two sided Mann-Whitney U test. **c)** Region of interest of one exemplary control and COVID-19 lung (as in a)), showing an overlay of the indicated markers. White arrows point out $IgA2^+CD27^+CD38^+$ cells. Scale bar: 20 µm. **(d-e)** Bronchoalveolar lavage (BAL) cells for single cell sequencing were enriched for $CD45^+$ cells via MACS and live cells were further sorted using FACS (see supplementary Fig. 4c). **d)** UMAP of 5459 cells representing clusters containing T cells, B cells and *CD14*-expressing cells from patient #1 on day 59 following ICU admission. B and T cell cluster identification based on BCR/TCR, *CD19*, *CD3E*, *CD4* and *CD8A* expression (see supplementary Fig. 4d). UMAP representation of expression of *TGFB1*, *IL21*, *CD40LG* and *IFNG*. **e)** UMAP coordinates and clustering was computed for 433 and 2723 cells from patient #9 on days 31 and 46 following ICU admission, respectively. UMAP representation of expression of *TGFB1*, *IL21*, *CD40LG* and *IFNG* at the two different time points is shown side by side.

Supplementary Figure 1. a) Demographics,disease history and serological information about S, its RBD domain and NP of SARS-CoV-2 of patients and healthy controls analyzed. **b)** Gating strategy used for FACS of activated B cells ($CD27^{high}$ $CD38^{high}$) from fresh peripheral blood of COVID-19 patients and healthy controls. Before FACS, cells were pre-enriched by MACS using StraightFrom® blood CD19 MicroBeads. **c)** Number of cells per donor present in each cluster. **d)** UMAP representation of the expression levels of selected activation/function, integrin, chemokine receptor and IL-21/STAT3 and TGF-β/SMADs signaling associated genes of sorted $CD27^{high}$ $CD38^{high}$ B cells from 9 COVID-19 ICU patients and 3 healthy controls (see Fig. 1b).

Supplementary Figure 2. a) Profiles of serum antibodies specific for SARS-Cov-2 S protein of COVID-19 patients. Representative dot plots of viable 293T cells transfected with either a SARS-CoV-2 S protein-expressing plasmid or mock transfected, incubated either with the recombinant anti-spike protein antibody (CR3022), as a control, or with serum (diluted 1:50 in PBS) of COVID-19 patients and healthy controls, and stained with fluorescently labelled anti-hIgG, anti-hIgA-FITC, anti-hIgM-PE, anti-hIgA1 or anti-hIgA2. **b)** Binding of IgG, IgM, IgA1 and IgA2 antibodies to SARS-CoV-2-S protein expressed on the surface of transfected 293T cells. Data represent ΔMFI, which was calculated as following: MFI (transfected cells, incubated with sera and stained with respective anti-hIgA1 or anti-hIgA2) – MFI (untransfected cells, incubated with sera and stained with respective anti-hIgA1 or anti-hIgA2). **c**) Binding of IgG, IgM, IgA1 and IgA2 antibodies to SARS-CoV-2-S-RBD

protein in COVID-19 ICU patients quantified by ELISA. When more than one time point per patient was available, the earliest time point was used. **d)** Binding of IgG, IgM, IgA1 and IgA2 antibodies to SARS-CoV-2-NP in COVID-19 ICU patients quantified by ELISA. When more than one time point per patient was available, the earliest time point was used. **e)** Correlation between SARS-CoV-2 S-RBD antibodies measured by ELISA versus antibodies binding to the Sars-CoV-2 S protein expressed on the surface of 293 T cells. Correlations for specific IgG and IgM antibodies were performed using sera from COVID-19 patients diluted 200 times, for IgA1 and IgA2 – sera was diluted 50 times. Spearman rank correlation was applied for analysis of correlations between ELISA- and flow cytometry- based antibody measurements. **f)** Concentration of total IgG and IgA1 in the serum of COVID-19 patients at early (less than a week) and late time points after ICU admission as determined by ELISA.

Supplementary Figure 3. a) UMAP representation of the expression of the Fc region of the inactive heavy Ig chain for individual cells transcribing two Ig heavy chain gene loci. Along with an active Ig heavy chain B cells can transcribe the inactive, allelically excluded, nonproductive IgH locus, starting from pseudoexons (I exons) before the switch regions, under the control of distinct cytokines as discussed above, and proceeding through the entire adjacent Ig constant region gene (germline/switch transcripts). Arrows represent the time patients had spent in intensive care at the time of analysis (upper) and the shift in cytokine milieu to allow switching to IgG1/IgA1/IgA2 (left). **b)** Correlation of Fc regions of the active and inactive heavy chain transcripts for COVID-19 patients. Shown are cell counts with identified two heavy chain transcripts: an active productive transcript, showing up to 100x higher expression and an inactive nonproductive IgH transcript. **c)** Gene Set Enrichment Analysis (GSEA) for IL-2/IL-21 and IL-6/IL-21/type I IFN-stimulation signature genes as defined by contrasting IL-2/IL-21-activated B cells and B cells with an additional IL-6/IL-21/type I IFN, IL-6/IL-21/TGF-β or IL-6/IL-21/type I IFN/TGF-β treatment for 12h. Signature genes were based on the gene expression data set published by Stephenson *et al.(Stephenson et al., 2019)* where peripheral blood B cells from healthy donors were differentiated in presence of IL-2 and IL-21, and subsequently stimulated with different cytokine cocktails during different time periods. GSEA was performed for each cell relative to the mean expression in COVID-19 and healthy control samples. Cells with statistically significant enrichments were color-scaled by the normalized enrichment score (NES), with red shades for cells showing up- and blue for cells showing down-regulation. UMAP was performed collectively with all COVID-19 and healthy samples and separated for visualization.

Supplementary Figure 4. a) Demographics, disease history and serological information about S, its RBD domain and NP of SARS-CoV-2 of patients and healthy controls analyzed. **b)** Flow cytometric analysis of SARS-CoV-2-reactive peripheral blood $CD4^+$ T cells from 3 COVID-19 ICU patients and 1 healthy control. For analysis, PBMCs were stimulated for 6 hours with anti-CD28 and a mixed peptide pool representing the SARS-CoV-2 spike glycoprotein (S), the membrane glycoprotein (M), and the nucleocapsid phosphoprotein (N) in presence of anti-CD40. Antigen-reactive regulatory T cells were identified by the upregulation of CD137, while antigen-reactive effector T cells were identified by the upregulation of CD154. This gating strategy was also used for cytometric sorting of $CD137^+$ and $CD154^+$ $CD4^+$ T cells for single cell transcriptomics and repertoire analysis. Staining for IFN-γ, IL-2 and TNF gated on $CD4^+CD154^+$ T cells. **c)** Effective number of clones (diversity)

of individual patients at different Hill orders. Hill order of 0 represents the observed number of different clonotypes. **d)** Clonal relatives of 6 selected clonal families from COVID-19 patients 6 (clone distribution in UMAP projection of activated B cell clusters and clonal tree), 5 and 4 (clonal trees only). A clonal family comprise clones with the same germline FR1-FR3 sequence, used V-, J- genes and the length of the cdr3 region in both heavy and light chain. Each pie chart represents at least one clone with a particular FR1-FR3 sequence. Numbers indicate the nucleotide differences (mutations) discriminating cells from their next common ancestor. Marked by red arrows are clones, from which the reconstructed BCR sequences were used to produce recombinant antibodies. These Antibodies were tested for binding to S and NP of SARS-CoV-2.

Supplementary Figure 5. a) Demographics and disease history of patients and controls of histologically analyzed autopsy cases. **b)** 5-marker MELC panel acquired in SARS-CoV2-positive lymph node and lung (COVID-19_A without and COVID-19_B with sepsis) and control lungs (SARS-CoV2 negative, bacterial infection due to aspiration pneumonia). Each image depicts the same field of view, sequentially stained with the depicted fluorescence-labelled antibodies and the nuclear stain DAPI. Magenta arrows point to $IgA2^{+}IgA^{+}CD27^{+}CD38^{+}$ cells (containing a nucleus). Images contain 2048 x 2048 pixels and are generated using an inverted wide-field fluorescence microscope with a 20x objective, a lateral resolution of 325 nm and an axial resolution above 5 µm. Scale bar: 100 µm. **c)** Gating strategy used for FACS of live $CD45^{+}$ cells from the BAL of COVID-19 patients. Before FACS, cells were pre-enriched by MACS using CD45 MicroBeads. **d)** UMAP representation of the expression of selected genes in the cells obtained from the BAL of patient #1 on day 59 following ICU admission (see Fig. 4d). Selected genes and BCR/TCR presence allow the identification of cell type belonging to each cluster **e)** UMAP representation of the expression of selected genes in the cells obtained from the BAL of patient #9 on days 31 and 46 following ICU admission (see Fig. 4e). Selected genes allow the identification of the cell types belonging to each cluster.

Figure 1

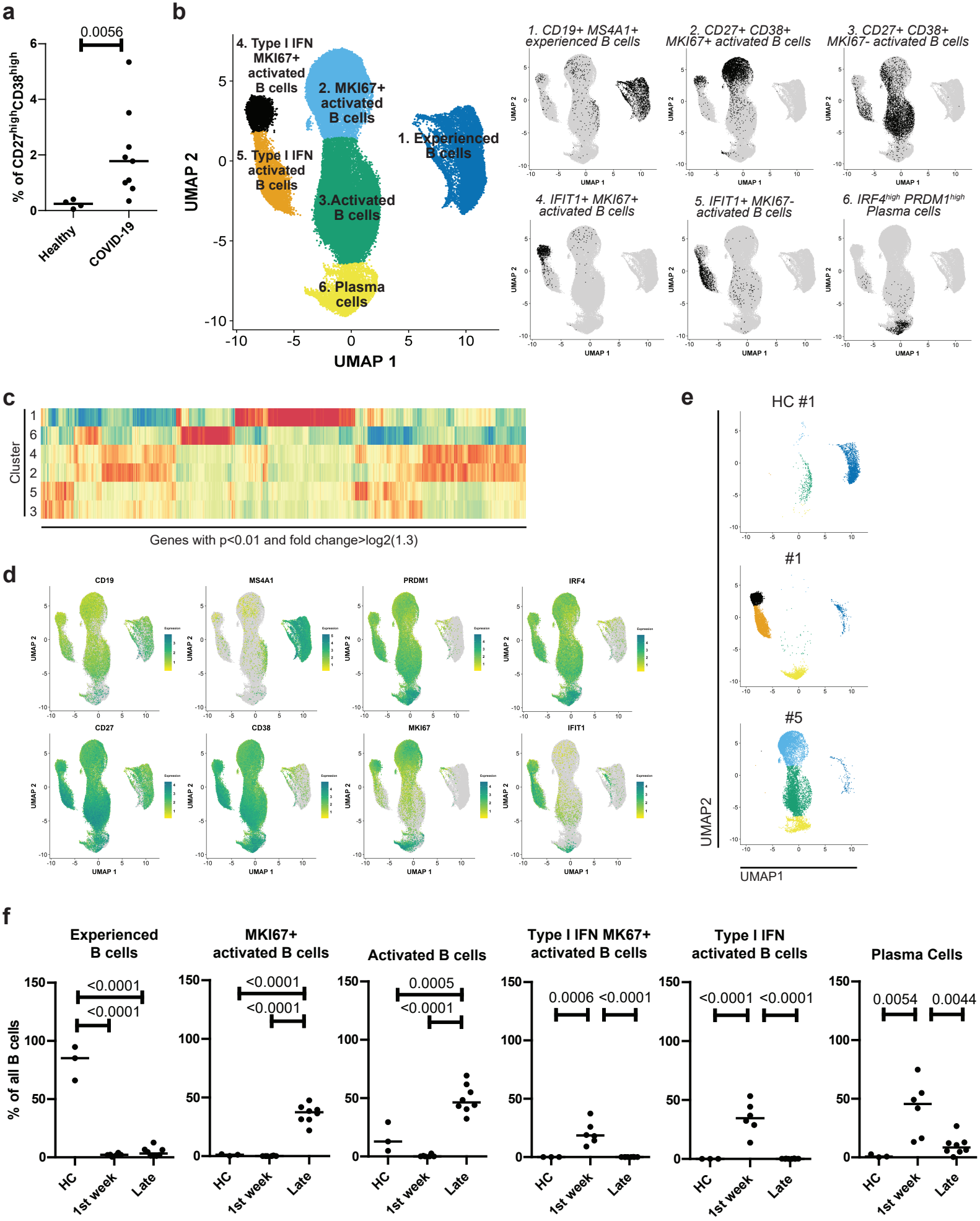
a
0.0056
% of CD27high CD38high
Healthy
COVID-19
b
4. Type I IFN MKI67+ activated B cells
2. MKI67+ activated B cells
1. Experienced B cells
5. Type I IFN activated B cells
3.Activated B cells
6. Plasma cells
UMAP 2
UMAP 1
1. CD19+ MS4A1+ experienced B cells
2. CD27+ CD38+ MKI67+ activated B cells
3. CD27+ CD38+ MKI67- activated B cells
4. IFIT1+ MKI67+ activated B cells
5. IFIT1+ MKI67- activated B cells
6. IRF4high PRDM1high Plasma cells
c
Cluster
1
6
4
2
5
3
Genes with p<0.01 and fold change>log2(1.3)
d
CD19
MS4A1
PRDM1
IRF4
CD27
CD38
MKI67
IFIT1
UMAP 2
UMAP 1
e
HC #1
#1
#5
UMAP2
UMAP1
f
Experienced B cells
MKI67+ activated B cells
Activated B cells
Type I IFN MK67+ activated B cells
Type I IFN activated B cells
Plasma Cells
% of all B cells
<0.0001
<0.0001
<0.0001
<0.0001
0.0005
<0.0001
0.0006
<0.0001
<0.0001
<0.0001
0.0054
0.0044
HC
1st week
Late

Figure 2

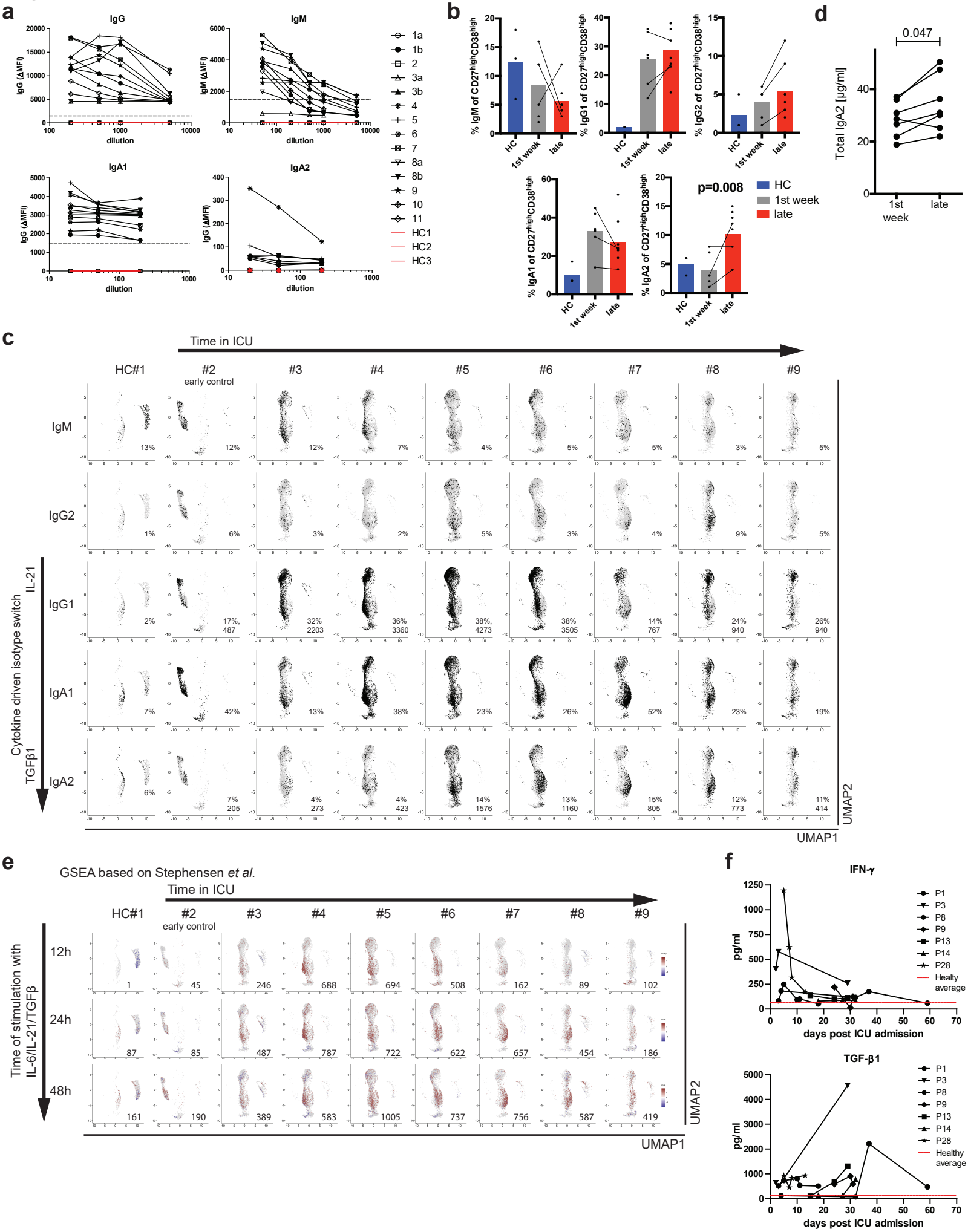
a
IgG
IgM
IgA1
IgA2
IgG (ΔMFI)
IgM (ΔMFI)
dilution
1a
1b
2
3a
3b
4
5
6
7
8a
8b
9
10
11
HC1
HC2
HC3
b
% IgM of CD27highCD38high
% IgG1 of CD27highCD38high
% IgG2 of CD27highCD38high
% IgA1 of CD27highCD38high
% IgA2 of CD27highCD38high
HC
1st week
late
p=0.008
d
0.047
Total IgA2 [µg/ml]
1st week
late
c
Time in ICU
HC#1
#2
early control
#3
#4
#5
#6
#7
#8
#9
IgM
IgG2
IgG1
IgA1
IgA2
Cytokine driven isotype switch
IL-21
TGFβ1
UMAP2
UMAP1
e
GSEA based on Stephensen et al.
Time in ICU
HC#1
#2
early control
#3
#4
#5
#6
#7
#8
#9
Time of stimulation with IL-6/IL-21/TGFβ
12h
24h
48h
UMAP2
UMAP1
f
IFN-γ
pg/ml
days post ICU admission
P1
P3
P8
P9
P13
P14
P28
Healty average
TGF-β1
pg/ml
days post ICU admission
P1
P3
P8
P9
P13
P14
P28
Healthy average

Figure 3

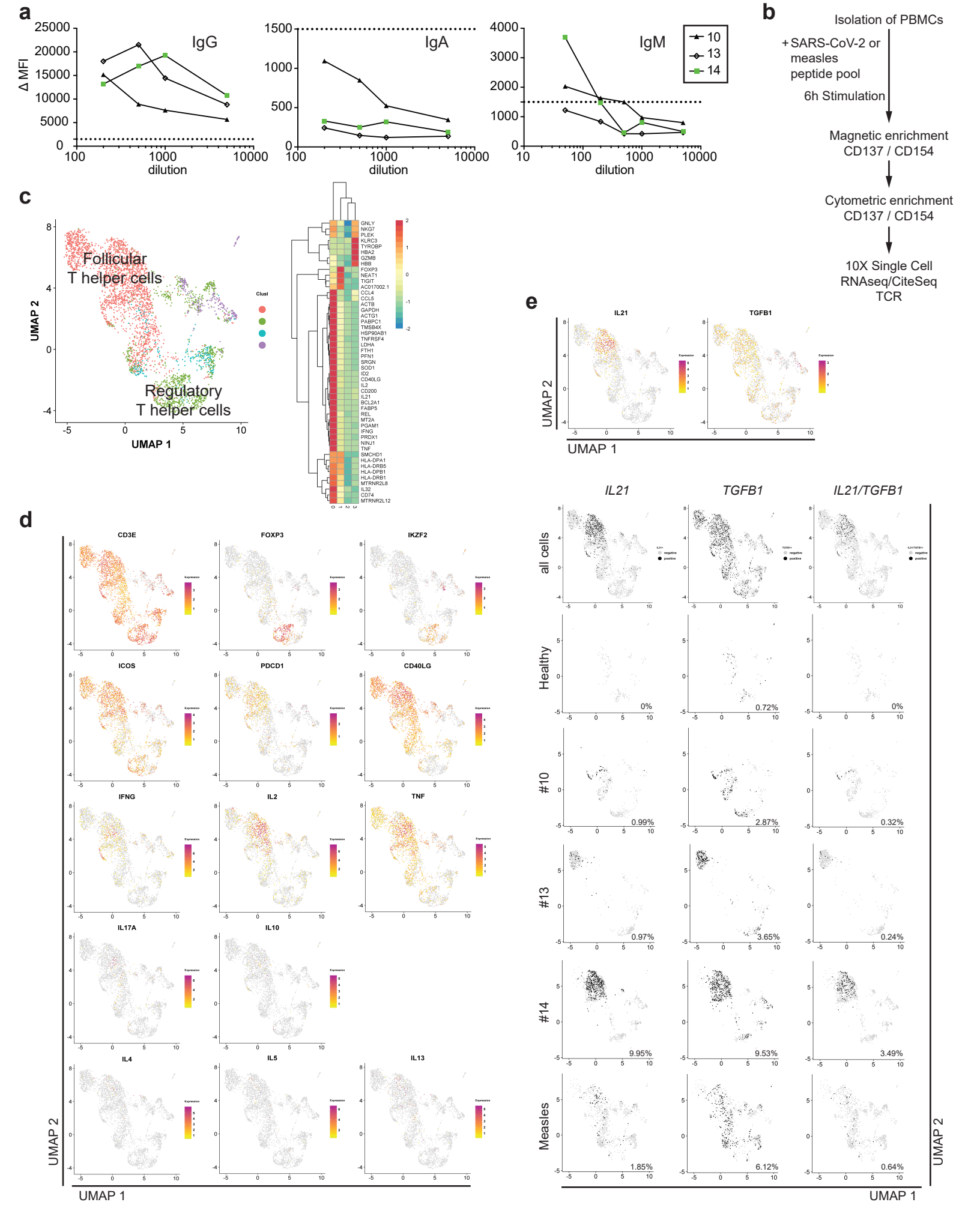
a
IgG
IgA
IgM
Δ MFI
dilution
10
13
14
b
Isolation of PBMCs
+ SARS-CoV-2 or measles peptide pool
6h Stimulation
Magnetic enrichment CD137 / CD154
Cytometric enrichment CD137 / CD154
10X Single Cell RNAseq/CiteSeq TCR
c
Follicular T helper cells
Regulatory T helper cells
UMAP 1
UMAP 2
Clust
GNLY
NKG7
PLEK
KLRC3
TYROBP
HBA2
GZMB
HBB
FOXP3
NEAT1
TIGIT
AC017002.1
CCL4
CCL5
ACTB
GAPDH
ACTG1
PABPC1
TMSB4X
HSP90AB1
TNFRSF4
LDHA
FTH1
PFN1
SRGN
SOD1
ID2
CD40LG
IL2
CD200
IL21
BCL2A1
FABP5
REL
MT2A
PGAM1
IFNG
PROX1
NINJ1
TNF
SMCHD1
HLA-DPA1
HLA-DRB5
HLA-DPB1
HLA-DRB1
MTRNR2L8
IL32
CD74
MTRNR2L12
d
CD3E
FOXP3
IKZF2
ICOS
PDCD1
CD40LG
IFNG
IL2
TNF
IL17A
IL10
IL4
IL5
IL13
e
IL21
TGFB1
IL21/TGFB1
all cells
Healthy
#10
#13
#14
Measles
0%
0.72%
0%
0.99%
2.87%
0.32%
0.97%
3.65%
0.24%
9.95%
9.53%
3.49%
1.85%
6.12%
0.64%

Figure 4

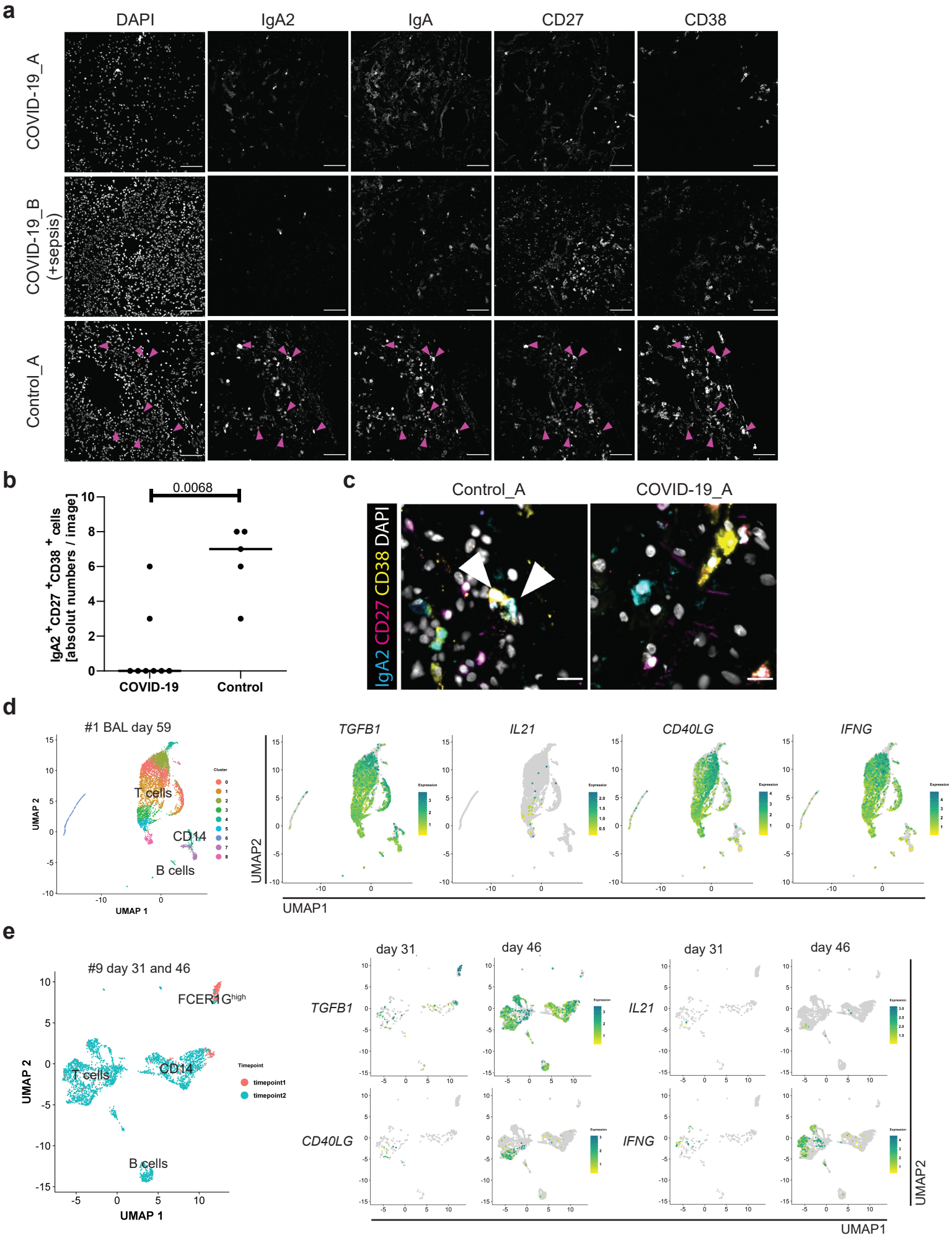
a
DAPI
IgA2
IgA
CD27
CD38
COVID-19_A
COVID-19_B (+sepsis)
Control_A
b
0.0068
IgA2 +CD27 +CD38 + cells [absolut numbers / image]
COVID-19
Control
c
Control_A
COVID-19_A
IgA2 CD27 CD38 DAPI
d
#1 BAL day 59
T cells
CD14
B cells
UMAP 1
UMAP 2
Cluster
TGFB1
IL21
CD40LG
IFNG
Expression
UMAP1
UMAP2
e
#9 day 31 and 46
FCER1G high
T cells
CD14
B cells
Timepoint
timepoint1
timepoint2
day 31
day 46
TGFB1
IL21
CD40LG
IFNG